Author/s:
Lin, G;Cortez-Jugo, C;Ju, Y;Besford, QA;Ryan, TM;Pan, S;Richardson, JJ;Caruso, F

Title:
Microemulsion-Assisted Templating of Metal-Stabilized Poly(ethylene glycol) Nanoparticles

Date:
2021-02-08

Citation:
Lin, G., Cortez-Jugo, C., Ju, Y., Besford, Q. A., Ryan, T. M., Pan, S., Richardson, J. J. & Caruso, F. (2021). Microemulsion-Assisted Templating of Metal-Stabilized Poly(ethylene glycol) Nanoparticles. Biomacromolecules, 22 (2), pp.612-619. https://doi.org/10.1021/acs.biomac.0c01463.

Persistent Link:
https://hdl.handle.net/11343/257662

Microemulsion-Assisted Templating of Metal-Stabilized Poly(ethylene glycol) Nanoparticles

Gan Lin,[†] Christina Cortez-Jugo,[†] Yi Ju,[†] Quinn A. Besford,[†,§] Timothy M. Ryan,[‡] Shuaijun Pan,[†] Joseph J. Richardson,[†] and Frank Caruso[†]*

[†]ARC Centre of Excellence in Convergent Bio-Nano Science and Technology, and the Department of Chemical Engineering, The University of Melbourne, Parkville, Victoria 3010, Australia

[§]Leibniz Institute for Polymer Research, Hohe Straße 6, 01069 Dresden, Germany

[‡]Australian Synchrotron, ANSTO, 800 Blackburn Rd., Clayton, Victoria 3168, Australia

ABSTRACT

Poly(ethylene glycol) (PEG) is well known to endow nanoparticles (NPs) with low-fouling and stealth-like properties that can reduce immune system clearance in vivo, making PEG-based NPs (particularly sub-100 nm) of interest for diverse biomedical applications. However, the preparation of sub-100 nm PEG NPs with controllable size and morphology is challenging. Herein, we report a strategy based on noncovalent coordination between PEG-polyphenolic ligands (PEG-gallol) and transition metal ions using a water-in-oil microemulsion phase to synthesize sub-100 nm PEG NPs with tunable size and morphology. The metal–phenolic coordination drives the self-assembly of the PEG-gallol/metal NPs: complexation between Mn^{II} and PEG-gallol within the microemulsions yields a series of metal-stabilized PEG NPs, including 30–50 nm solid and hollow NPs, depending on the Mn^{II}:gallol feed ratio. Variations in size and morphology are attributed to changes in hydrophobicity of the PEG-gallol/Mn^{II} complexes at varying Mn^{II}:gallol ratios based on contact angle measurements. Small-angle X-ray scattering analysis, which is used to monitor particle size and intermolecular interactions during NP evolution, reveals that ionic interactions are the dominant driving force in the formation of the PEG-gallol/Mn^{II} NPs. pH and cytotoxicity studies, and the low-fouling properties of the PEG-gallol/Mn^{II} NPs confirm their high biocompatibility and functionality, suggesting that PEG polyphenol–metal NPs are promising systems for biomedical applications.

KEYWORDS: Metal–organic coordination, soft templating, PEG nanoparticles, pH-responsive

1. INTRODUCTION

In recent years, a variety of nanocarriers with broad functional properties have been developed to encapsulate therapeutic and/or imaging agents for applications in nanomedicine.[1–3] However, their success in vivo is limited by biological barriers, including the mononuclear phagocyte system (MPS), which serves to clear foreign bodies by opsonization for uptake and clearance by phagocytic cells.[4,5] Opsonization involves the adsorption of proteins, including antibody receptors and complement proteins, on the particle surface to facilitate recognition by the immune system for clearance. Hence, the engineering of particles that can display reduced protein adsorption capacity on their surface has been a major focus in particle design. As a common strategy to address this challenge is the use of low-fouling materials in particle synthesis or as a coating on the particle surface. Of particular relevance is the use of poly(ethylene glycol) (PEG), which is a widely applied polymer in many particle assemblies.[6,7] The hydrophilic properties and neutral charge of PEG afford reduced protein interactions through a shielding hydration layer of water,[8] thereby inhibiting immune system recognition and uptake by the MPS to thus achieve enhanced circulation of the therapeutic-loaded carrier and subsequent effective target accumulation.[9]

To exploit the prolonged blood circulation and reduced phagocytic uptake of PEG-based drug delivery carriers, several methods have been developed to construct particles composed primarily of PEG.[10–15] For example, a high-throughput method by combining photolithography and microfluidics to produce micrometer-sized PEG particles with precise control over size, shape, and aspect ratio has been reported.[10] In addition, a particle replication in nonwetting template technique has been developed for preparing hydrogel PEG particles with controlled shape, size, and surface chemistry.[11] We also reported the synthesis of PEG-based polymer capsules via layer-by-layer assembly and recently developed a mesoporous silica templating method to

engineer hydrogel PEG particles.[12–18] The potential for a broad range of biomedical applications, including tumor targeting, has been demonstrated for long-circulating hydrogel PEG particles.[16,17] Although the templating method resulted in PEG particles with tunable mechanical properties (elasticity) and controllable particle size,[14,18] the techniques for PEG particle assembly have been largely limited to preparing large (>100 nm) particles. However, PEG particles of <100 nm in size, the synthesis of which is challenging, are considered a more suitable size for a range of intravenous drug delivery applications.[19] Therefore, there is a need to develop facile methods that can afford sub-100 nm PEG particles for biological applications.

As a potential approach, we reported the fabrication of PEG particles and capsules based on the inorganic coordination between transition metal ions and phenolic gallol groups within PEG-polyphenolic ligands.[20–23] This coordination is the basis of the formation of metal–phenolic network (MPN) films on various planar and colloidal substrates.[24,25] MPN particles, including capsules, have been investigated for various applications, including catalysis, drug delivery, medical imaging, and pulmonary delivery.[26] Functionalization of PEG with catechols to form PEG-polyphenols allows the formation of functional metal ion-complexed PEG-based MPN films on various substrates such as calcium carbonate (>2 μm) and microemulsions (~100–250 nm in size).[21–23]

Herein, the coordination between PEG-polyphenol (PEG-gallol) and metal ions (Fe^{III} or Mn^{II}) within a water-in-oil emulsion system was exploited to synthesize metal-stabilized PEG nanoparticles (NPs). By varying the Mn^{II}:gallol ratio, NPs with different sizes (<100 nm) and morphologies (solid vs hollow) were obtained, whereas varying the Fe^{III}:gallol ratio consistently resulted in 30 nm solid PEG-gallol/Fe^{III} NPs. The mechanism behind the formation of the PEG-gallol/Mn^{II} NPs and their evolution into different sizes and morphologies were investigated by

small-angle X-ray scattering (SAXS) and contact angle measurements, respectively. Finally, the low-fouling behavior of the PEG-gallol/Mn^{II} hollow NPs, as well as their biocompatibility and drug release properties were determined to demonstrate their potential as a therapeutic particle system.

2. EXPERIMENTAL SECTION

2.1. Materials

Manganese(II) chloride tetrahydrate ($MnCl_2 \cdot 4H_2O$), tris-(hydroxymethyl)aminomethane (TRIS), ethanol, tetrahydrofuran (THF), thiazolyl blue tetrazolium bromide (MTT), cyclohexane, Triton X-100, 1-hexanol, and radioimmunoprecipitation (RIPA) lysis buffer were purchased from Sigma-Aldrich and used as received without further purification. 8-Arm-poly(ethylene glycol) succinimidyl succinate (8-arm-PEG-NHS, hexaglycerol core, molecular weight 10 kDa) was purchased from JenKem Technology (USA). Multi-element ICP standard solutions and nitric acid (ultrapure) for inductively coupled plasma–optical emission spectroscopy (ICP-OES) analysis were purchased from Merck KGaA (Germany). Dulbecco's Modified Eagle Medium (DMEM), Roswell Park Memorial Institute medium (RPMI), fetal bovine serum (FBS), and Dulbecco's phosphate-buffered saline (PBS) were purchased from Life Technologies. High-purity (Milli-Q) water was obtained from an inline Millipore RiOs/Origin water purification system.

2.2. Synthesis of PEG-Gallol/Fe^{III} and PEG-Gallol/Mn^{II} NPs by Microemulsion Templating

PEG-gallol was first synthesized according to our previous method.[21,23] The PEG-gallol/Mn^{II} (or PEG-gallol/Fe^{III}) NPs were then prepared by reverse microemulsion using a reported protocol with minor modifications.[27] Briefly, 200 μL of a mixture of aqueous $MnCl_2 \cdot 4H_2O$ (or

$FeCl_3 \cdot 6H_2O$) solution and PEG-gallol (5 mg mL^{-1}) was added into a 5 mL of 0.3 M Triton X-100/1.5 M 1-hexanol mixture in cyclohexane under vigorous stirring in a 15 mL vial at room temperature. After 20 min of stirring, a further 5 mL of 0.3 M Triton X-100/1.5 M 1-hexanol mixture in cyclohexane containing 200 µL TRIS buffer (pH 8.0) was added to raise the pH of the mixture for cross-linking. After 30 min of stirring, the microemulsion mixture was transferred into a 50 mL tube containing 10 mL ethanol. The solution was sonicated for 5 min, then transferred into 2 mL tubes for centrifugation (7000*g*, 5 min) to obtain PEG-gallol/Mn^{II} (or PEG-gallol/Fe^{III}) NP pellets. The NPs were washed with 1.5 mL 50% (v/v) ethanol/cyclohexane in 2 mL tubes, spun down by centrifugation (7000*g*, 5 min) and the supernatant was removed. The NPs were washed further with 1.5 mL 50% (v/v) ethanol/THF and then with 1.5 mL ethanol, using the same centrifugation conditions. Finally, the PEG-gallol/Mn^{II} or PEG-gallol/Fe^{III} NPs were dispersed in Milli-Q water until further analysis.

2.3. Characterization of PEG-Gallol/Fe^{III} and PEG-Gallol/Mn^{II} NPs

Dynamic light scattering (DLS) measurements were conducted to measure the hydrodynamic diameter of the particles using a Zetasizer Nano ZS instrument (Malvern Instruments, Malvern, UK). Transmission electron microscopy (TEM) and element mapping, via energy-dispersive X-ray spectroscopy, of the PEG-gallol/metal NPs were performed on an FEI Tecnai F20 transmission electron microscope operating at an acceleration voltage of 200 kV. Ultraviolet–visible (UV–vis) spectroscopy was conducted on a Cary 4000 UV–vis spectrophotometer (Agilent Technologies, USA). The concentration of Mn in the PEG-gallol/Mn^{II} NPs was determined by ICP-OES on a Varian 720-ES inductively coupled plasma–optical emission spectrometer (Agilent, USA). The NPs were decomposed in 1 M HCl solutions, and the metal concentration was determined against a standard curve of Mn at known concentrations.

2.4. Contact Angle Measurements

Contact angle measurements were carried out on a DataPhysics OCA 20 tensiometer. Briefly, 5 μL of a water droplet containing PEG-gallol/Mn^{II} complexes (concentration of PEG-gallol: 1 mg mL^{-1}) with varying Mn^{II}:gallol ratios was pipetted onto a clean glass substrate and allowed to air dry. The contact angle of pure water on the deposited PEG-gallol/Mn^{II} complex/film was then measured.

2.5. In Situ SAXS Studies

In situ SAXS experiments were performed to monitor the metal–phenolic coordination-driven PEG particle formation at the Australian Synchrotron (SAXS beamline). The experiment was performed using a 7 m camera setup with a Pilatus2 1 M detector in a pulsed pumping mode to increase the statistics over a large volume of solution. Upon mixing of the two microemulsion solutions (one containing PEG-gallol/Mn^{II} and one containing TRIS buffer (pH 8.0)), the SAXS patterns were measured within a 1.5 mm Quartz capillary tube and collected every 10 min. The SAXS data were fitted using Igor 6 analysis software (WaveMetrics Inc., Lake Oswego, OR, USA). The ionic screening model (Hayter–Penfold model) was used to fit the interparticle interaction. The ionic screening model fits an interaction distance and a concentration of ions on screening (**Table S1**) and assumes a standard dielectric constant and charged particles, which was estimated from the molecular formula and pH.

2.6. Release Profiles of PEG-Gallol/Mn^{II} Hollow NPs

The release study was conducted according to our previously established protocol.[21] Briefly, the PEG-gallol/Mn^{II} hollow NPs (an aliquot of 100 μL containing 26.4 μg Mn^{II} according to ICP-OES measurements) were dialyzed against 10 mL PBS buffer (10 mM, pH 5.5 or 7.4) using a dialysis membrane with a molecular weight cutoff of 3500 Da. At each pre-determined time

point, 5 mL of the dialysis solution containing released Mn^{II} ions was withdrawn and replaced with the same volume of fresh buffer. The concentration of Mn^{II} was then determined by ICP-OES using a standard curve of Mn^{II} ions.

2.7. Cell Viability Assays

RAW 264.7 cells were plated on a 96-well plate (Costar 3596, Corning, MA, USA) at a cell density of 5000 cells per well in 100 μL DMEM supplemented with 10% FBS. After incubation for 12 h at 37 °C with 5% CO_2, the PEG-gallol/Mn^{II} hollow NPs were added to the cells at varying concentrations (equivalent to 0.05, 0.1, 0.2, 0.5, 1, 2, and 5 μM Mn^{II}). After incubation of the particles with the cells for 24 h, the cell viability was evaluated by the MTT assay. The absorbance at 570 nm was recorded using an Infinite M200 microplate reader. The cell viability was normalized against the absorbance obtained from nontreated cells.

2.8. Cell Association by ICP

Raw 264.7 and HeLa cells were maintained in DMEM supplemented with 10% FBS at 37 °C with 5% CO_2. Jurkat cells were maintained in RPMI media supplemented with 10% FBS at 37 °C with 5% CO_2. To assess cell association, Raw 264.7, HeLa, and Jurkat cells were seeded into 6-well plates at a density of 5×10^5 cells per well and incubated overnight at 37 °C with 5% CO_2. PEG-gallol/Mn^{II} hollow NPs corresponding to a Mn^{II} concentration of 5 μM were added to the cells and incubated for 1, 2, 4, 8, and 24 h at 37 °C with 5% CO_2. After incubation, the cell culture media was removed and the Raw 264.7 and HeLa cells were washed with PBS thrice and then collected using a cell scraper, followed by centrifugation at 1000*g* for 5 min. The Jurkat cells were directly spun down (1000*g*, 5 min) following NP incubation. Cells were lysed in RIPA lysis buffer and then incubated in aqua regia overnight. The samples were diluted with

concentrated nitric acid solution (2–3% by volume) and subjected to ICP-OES measurement for metal concentration determination.

3. RESULTS AND DISCUSSION

PEG-gallol was first synthesized by conjugating gallol groups onto the terminus of 8-arm-PEG (10 kDa) according to a previously reported method with minor modification (**Figure S1**).[21,23] Mixing of PEG-gallol with aqueous $FeCl_3$ or $MnCl_2$ solution and subsequent addition into an oil phase containing cyclohexane, hexanol, and Triton X-100 surfactant resulted in water-in-oil microemulsions containing PEG-gallol/Fe^{III} or PEG-gallol/Mn^{II} complexes. Raising the pH, by the addition of Tris buffer (pH 8.0) to the mixture, initiated metal–phenolic coordination within the microemulsions. PEG-gallol/Fe^{III} or PEG-gallol/Mn^{II} NPs were obtained after 1 h of stirring and subsequent washing with ethanol to remove the micelle templates and water for purification. The resulting metal-stabilized PEG NPs were characterized by DLS and TEM.

Complexing PEG-gallol with Fe^{III} resulted in solid NPs of ~30 nm in size regardless of the Fe^{III}:gallol ratio (**Figure S2**). This consistency in size regardless of the feed ratio is likely due to the strong affinity between gallols and Fe^{III} ions that results in instantaneous cross-linking of the PEG-gallol/Fe^{III} complexes within the microemulsions. In contrast, complexing PEG-gallol with Mn^{II} ions gave rise to PEG-gallol/Mn^{II} NPs of varying sizes and morphologies depending on the Mn^{II}:gallol feed ratio (**Scheme 1**). **Figure 1**a shows TEM images of the PEG-gallol/Mn^{II} NPs prepared using different Mn^{II}:gallol molar ratios (0.25:1, 1:1, 4:1). At a low feed ratio (i.e., 0.25:1; when the amount of gallol groups is excessively higher than that of Mn^{II}), small (~30 nm) solid PEG-gallol/Mn^{II} NPs were obtained (**Figure S3**). Increasing the feed ratio to 1:1 yielded larger solid NPs (~50 nm), whereas increasing the feed ratio to 4:1 resulted in large hollow NPs (~50 nm), which were similar in size as the micelle-stabilized (Triton X-100) microemulsions

(**Figures S3, S4**). The particle size distributions of the PEG-gallol/Mn^{II} NPs are shown in **Figure S3**. To improve reproducibility, reporting, and re-analysis, this study conforms to the Minimum Information Reporting in Bio–Nano Experimental Literature (MIRIBEL) standard,[28] and a companion checklist is provided in the Supporting Information.

UV–Vis absorbance spectroscopy was employed to investigate the interaction between the metal and PEG ligands in the PEG NPs. The spectra of the PEG-gallol/Mn^{II} NPs featured a new absorption peak in the range of 350–600 nm, which was absent in the spectrum of free PEG-gallol (**Figure 1**b). This new peak was attributed to the ligand-to-metal charge-transfer (LMCT) band of gallol/Mn^{II},[25] indicating the presence of gallol–Mn^{II} coordination in the PEG NPs. Bis- to tris-type coordination was previously reported for PEG-gallol/Fe^{III} films based on the LMCT band at 520 nm.[23] It is estimated that a bis- to tris-type coordination between Mn^{II} and PEG-gallol also occurs, indicating an approximate Mn^{II}:gallol binding ratio of 1:2 assuming most available groups interact with the metal centers. X-ray diffraction (XRD) studies were performed to determine the crystallinity of the PEG-gallol/Mn^{II} NPs. As observed from **Figure 1**c, the PEG-gallol/Mn^{II} NPs featured an XRD pattern similar to that of pure water and no crystalline peaks were observed. These data indicated that the PEG-gallol/Mn^{II} NPs were composed of amorphous metal–phenolic-driven PEG cross-linking.

In recent studies, it has been reported that the hydrophobicity/hydrophilicity of the precursor greatly affects the distribution of the monomer during emulsion formation, which can influence the morphology of the resulting particles.[29] To determine the hydrophobicity of the PEG-gallol/Mn^{II} complexes prepared at different feed ratios, contact angle measurements were performed on planar films of adsorbed PEG-gallol/Mn^{II} complexes at different Mn^{II}:gallol ratios. A droplet of pure water was placed on each film. As observed in **Figure 2**a, the water contact

angle increased from 12° to 19° and 44° as the Mn^{II}:gallol molar ratio increased from 0.25:1 to 1:1 and 4:1, respectively (**Figure 2**b). These results indicate an increase in hydrophobicity of the PEG-gallol/Mn^{II} complexes prepared at increasing Mn^{II} concentrations, thereby suggesting that different feed ratios resulted in varying cross-linking degrees in the PEG-gallol/Mn^{II} complexes, as illustrated in **Figure 2**c. At low Mn^{II} concentrations (e.g., Mn^{II}:gallol ratio of 0.25:1), the extent of metal–phenolic cross-linking is low so the PEG-gallol/Mn^{II} complexes remain hydrophilic and the complexes remain within the core of the water droplet. As the Mn^{II} concentration increases (Mn^{II}:gallol 1:1), the extent of metal–phenolic cross-linking increases, resulting in increases in the PEG cross-linking and hydrophobicity of the PEG-gallol/Mn^{II} complexes. This allows the PEG-gallol/Mn^{II} complexes to diffuse toward the water–oil interface, thus leading to larger particles. Increasing the Mn^{II} concentration further (Mn^{II}:gallol 4:1) increased the hydrophobicity of the PEG-gallol/Mn^{II} complexes further, thus confining the complexes to the water–oil interface.[30] Despite this being thermodynamically unfavorable, the higher PEG cross-linking density at Mn^{II}:gallol 4:1 likely freezes the PEG-gallol/Mn^{II} complexes at the interface and limits the chain mobility of the PEG, thereby leading to capsule-like structures. In addition, the increase in the ionic strength of the complexes, as a result of the increase in Mn^{II} concentration, could possibly contribute to the diffusion of the complexes to the water–oil interface. High ionic strength has been shown to lead to thicker and rougher metal–phenolic, e.g., tannic acid/Fe^{III}, films as the gallol groups on TA extend outward from the Fe^{III} center.[31] In the present study, the extension of gallol groups from the center of the PEG-gallol/Mn^{II} complexes at high ionic strength could potentially contribute to the dispersion of the complexes toward the water–oil phase, hence leading to larger and capsule-like structures.

In situ SAXS analysis was used to monitor the structural evolution of the PEG NPs within the microemulsions during the cross-linking reaction (**Figure** 3). As observed from **Figure 3**a, the intensity at the higher q values (0.08–0.09 $Å^{-1}$), corresponding to small PEG-gallol or PEG-gallol/Mn^{II} species, decreased as the reaction proceeded, suggesting the consumption of free small PEG-gallol/Mn^{II} complexes. In contrast, the intensity at the lower q values (0.001 $Å^{-1}$), which was assigned to large PEG-gallol/Mn^{II} particles (50–100 nm), increased with time, indicating an increase in the formation of larger particles as the reaction progressed. These SAXS results suggest that the small free PEG-gallol/Mn^{II} complexes convert into PEG-gallol/Mn^{II} particles during the reaction. The SAXS data at the reaction endpoint (60 min) were fitted with Igor 6 analysis software to model interparticle interaction. The Hayter–Penfold ionic screening model gave the best fitting, suggesting that ionic charges on the particles drive their self-assembly in solution. As summarized in **Table S1**, there was a significant increase in ion concentration from low to high Mn^{II}:gallol ratios, which is consistent with our experimental data. The size (diameter) of the small species in all three NP systems (low, medium, and high Mn^{II}:gallol ratio) was ~5 nm (**Figure 3**b), which can be assigned to free PEG-gallol or PEG-gallol/Mn^{II} complexes. The size of the large species was around 40–50 nm in the medium- and high-ratio NP systems (**Figure 3**c). These results agree with our TEM and DLS data (**Figure 1**a, **Figure S3**), indicating that some small PEG-gallol/Mn^{II} complexes polymerize into large PEG-gallol/Mn^{II} NPs over time. The large species in the low-ratio NP system (**Figure 3**c) were 90 nm in size, which is significantly larger than the actual size of the NPs observed by TEM and DLS. The larger size likely corresponds to aggregates of smaller particles formed during the reaction.

Given the well-recognized stealth properties of PEG and the capacity of sub-100 nm particles to enhance circulation times and cell uptake,[19,32] we examined the potential of the 50 nm PEG-

gallol/Mn^{II} hollow NPs as therapeutic particles by investigating their biocompatibility and stability at physiological pH. The hollow NPs were assessed because of their higher capacity for drug loading. The stability of the PEG-gallol/Mn^{II} hollow NPs was investigated in phosphate buffered saline (PBS) at pH values of 7.4 and 5.5. The release of the Mn^{II} ions, which results from the disassembly of the hollow NPs, was quantified by inductively coupled plasma–optical emission spectroscopy (ICP-OES) using standard curves of Mn^{II} ions (**Figure S5**). **Figure 4**a shows that only 3% of the Mn^{II} ions were released from the PEG-gallol/Mn^{II} hollow NPs when incubated in PBS at pH 7.4 for 8 h, demonstrating the stability of the PEG-gallol/Mn^{II} hollow NPs at that pH. In contrast, at pH 5.5, the hollow NPs displayed a considerably faster release profile (**Figure 4**a). Approximately 40% of the Mn^{II} ions were released at 8 h, after which time a sustained release was observed with a final release of 50% Mn^{II} at 24 h. Comparison of the hollow NPs at pH 7.4 and 5.5 by TEM confirmed the disassembly of the NPs at pH 5.5 (**Figure S6**) as evidenced by the reduction in the number of particles present at pH 5.5. The pH-sensitive properties of the metal-stabilized PEG hollow NPs afford a potentially promising drug delivery system that can prevent premature release of therapeutics during blood circulation but enable the release of the loaded cargo upon exposure to acidic disease sites, such as in tumors and inflammation sites, or after internalization into endosomes.[33–35] The biocompatibility of the PEG-gallol/Mn^{II} hollow NPs was demonstrated using a thiazolyl blue tetrazolium bromide cell viability assay. As shown in **Figure 4**b, when incubated with the macrophage cell line RAW 264.7 for 24 h at 37 °C, the PEG-gallol/Mn^{II} hollow NPs exhibited negligible cytotoxicity at Mn^{II} concentrations of less than 1 μM. This also suggests that there was negligible emulsion-stabilizing surfactant left on the particles that could cause cell death by membrane disruption. At the higher Mn^{II} concentrations corresponding to an increase in particle dosage (>1 μM Mn^{II} per

5000 cells), the PEG-gallol/Mn^{II} hollow NPs showed slight cytotoxicity, which may be due to the release of Mn^{II} ions when the capsules are internalized and disassemble in the acidic endosomal compartments. An accumulation of intracellular Mn has been associated with the production of reactive oxygen species that can induce cell death.[36]

PEG-based NPs have been reported to be low fouling and exhibit reduced nonspecific interactions with cells.[20,21] To assess the low-fouling properties of the PEG-gallol/Mn^{II} NPs, three different cell lines (RAW 264.7, HeLa, and Jurkat as models of macrophages, epithelial tumor cells, and T cells, respectively) were treated with the three different PEG-gallol/Mn^{II} NP systems at a dosage corresponding to 5 μM Mn^{II}. After incubation for 24 h at 37 °C in 5% CO_2, the cells were washed and harvested for ICP-OES analysis to determine the cellular Mn^{II} concentration for assessing the level of cellular association of the NPs. As indicated in **Figure 4**c, all three NP systems exhibited low fouling properties toward all three cell lines (<2% of cells had associated NPs). For comparison, MPN particles prepared from Fe^{III} and tannic acid as the polyphenol have shown high association with HeLa cells, with approximately 70% of cells having bound or internalized particles after incubation for 24 h at 37 °C.[21] Taken together, these results indicate that the currently engineered metal-stabilized PEG NPs are low fouling, which may reduce protein adsorption and opsonization, and hence clearance by the MPS.

4. CONCLUSIONS

We have developed a facile method to tune the size and morphology of metal-stabilized PEG NPs by controlling the metal-to-ligand ratio in the metal–phenolic complexes within water-in-oil microemulsions. Complexing of Mn^{II} and PEG-gallol gave rise to a series of metal-stabilized PEG NPs with varying size (30–50 nm) and morphology (solid or hollow). UV–Vis spectroscopy and XRD data indicated that PEG particle formation was driven by metal–phenolic coordination.

The difference in size and morphology was attributed to the variation in hydrophobicity of the PEG-gallol/Mn^{II} complex under different reaction ratios, as evidenced by contact angle measurements. SAXS data suggested that ionic charges are likely the dominant driving force in the evolution of PEG-gallol/Mn^{II} complexes into different PEG NPs. Finally, we showed that the metal-stabilized PEG NPs are highly biocompatible and possess low-fouling and pH-responsive properties that are important features for use as therapeutic NPs.

ASSOCIATED CONTENT

Supporting Information. Structure factors used in SAXS data fitting analysis (Igor 6) for microemulsion systems; ^{1}H-NMR spectrum of PEG-gallol in D_2O; DLS analysis; TEM images and UV–Vis spectra of PEG-gallol/Fe^{III} and PEG-gallol/Mn^{III} NPs; ICP-OES characterization; TEM images of PEG-gallol/Mn^{II} hollow NPs in PBS at pH 7.4 and pH 5.5; MIRIBEL checklist including material characterization, biological characterization, and experimental details.

AUTHOR INFORMATION

Corresponding Author

*E-mail: fcaruso@unimelb.edu.au (F.C.)

ACKNOWLEDGMENTS

This research was conducted and funded by the Australian Research Council Centre of Excellence in Convergent Bio-Nano Science and Technology (project number CE140100036). F.C. acknowledges the award a National Health and Medical Research Council Senior Principal Research Fellowship (GNT1135806). This work was performed in part at the Materials Characterisation and Fabrication Platform (MCFP) at The University of Melbourne and the

Victorian Node of the Australian National Fabrication Facility (ANFF). Part of this research was conducted at the SAXS beamline at the Australian Synchrotron.

REFERENCES

1. Cui, J.; Richardson, J. J.; Björnmalm, M.; Faria, M.; Caruso, F. Nanoengineered Templated Polymer Particles: Navigating the Biological Realm. *Acc. Chem. Res.* **2016**, *49*, 1139–1148.

2. Torchilin, V. P. Multifunctional, Stimuli-Sensitive Nanoparticulate Systems for Drug Delivery. *Nat. Rev. Drug Discovery* **2014**, *13*, 813–827.

3. Lin, G.; Mi, P.; Chu, C.; Zhang, J.; Liu, G. Inorganic Nanocarriers Overcoming Multidrug Resistance for Cancer Theranostics. *Adv. Sci.* **2016**, *3*, 1600134.

4. Blanco, E.; Shen, H.; Ferrari, M. Principles of Nanoparticle Design for Overcoming Biological Barriers to Drug Delivery. *Nat. Biotechnol.* **2015**, *33*, 941–951.

5. Tsoi, K. M.; MacParland, S. A.; Ma, X.-Z.; Spetzler, V. N.; Echeverri, J.; Ouyang, B.; Fadel, S. M.; Sykes, E. A.; Goldaracena, N.; Kaths, J. M.; Conneely, J. B.; Alman, B. A.; Selzner, M.; Ostrowski, M. A.; Adeyi, O. A.; Zilman, A.; McGilvray, I. D.; Chan, W. C. W. Mechanism of Hard-Nanomaterial Clearance by the Liver. *Nat. Mater.* **2016**, *15*, 1212–1221.

6. Suk, J. S.; Xu, Q.; Kim, N.; Hanes, J.; Ensign, L. M. PEGylation as a Strategy for Improving Nanoparticle-Based Drug and Gene Delivery. *Adv. Drug Delivery Rev.* **2016**, *99*, 28–51.

7. Jokerst, J. V.; Lobovkina, T.; Zare, R. N.; Gambhir, S. S. Nanoparticle PEGylation for Imaging and Therapy. *Nanomedicine* **2011**, *6*, 715–728.

8. Zhang, K.; Huang, H.; Hung, H.-C.; Leng, C.; Wei, S.; Crisci, R.; Jiang, S.; Chen, Z. Strong Hydration at the Poly(ethylene glycol) Brush/Albumin Solution Interface. *Langmuir* **2020**, *36*, 2030–2036.

9. Harris, J. M.; Chess, R. B. Effect of pegylation on pharmaceuticals. *Nat. Rev. Drug Discovery* **2003**, *2*, 214–221.

10. Dendukuri, D.; Pregibon, D. C.; Collins, J.; Hatton, T. A.; Doyle, P. S. Continuous-Flow Lithography for High-Throughput Microparticle Synthesis. *Nat. Mater.* **2006**, *5*, 365–369.

11. Xu, J.; Wong, D. H. C.; Byrne, J. D.; Chen, K.; Bowerman, C.; DeSimone, J. M. Future of the Particle Replication in Nonwetting Templates (PRINT) Technology. *Angew. Chem. Int. Ed.* **2013**, *52*, 6580–6589.

12. Leung, M. K. M.; Such, G. K.; Johnston, A. P. R.; Biswas, D. P.; Zhu, Z.; Yan, Y.; Lutz, J.-F.; Caruso, F. Assembly and Degradation of Low-Fouling Click-Functionalized Poly(ethylene glycol)-Based Multilayer Films and Capsules. *Small* **2011**, *7*, 1075–1085.

13. Yap, H. P.; Johnston, A. P. R.; Such, G. K.; Yan, Y.; Caruso, F. Click-Engineered, Bioresponsive, Drug-Loaded PEG Spheres. *Adv. Mater.* **2009**, *21*, 4348–4352.

14. Cui, J.; Björnmalm, M.; Liang, K.; Xu, C.; Best, J. P.; Zhang, X.; Caruso, F. Super-Soft Hydrogel Particles with Tunable Elasticity in a Microfluidic Blood Capillary Model. *Adv. Mater.* **2014**, *26*, 7295–7299.

15. Cui, J.; De Rose, R.; Alt, K.; Alcantara, S.; Paterson, B. M.; Liang, K.; Hu, M.; Richardson, J. J.; Yan, Y.; Jeffery, C. M.; Price, R. I.; Peter, K.; Hagemeyer, C. E.; Donnelly, P.

S.; Kent, S. J.; Caruso, F. Engineering Poly(ethylene glycol) Particles for Improved Biodistribution. *ACS Nano* **2015**, *9*, 1571–1580.

16. Cui, J.; Ju, Y.; Houston, Z. H.; Glass, J. J.; Fletcher, N. L.; Alcantara, S.; Dai, Q.; Howard, C. B.; Mahler, S. M.; Wheatley, A. K.; De Rose, R.; Brannon, P. T.; Paterson, B. M.; Donnelly, P. S.; Thurecht, K. J.; Caruso, F.; Kent, S. J. Modulating Targeting of Poly(ethylene glycol) Particles to Tumor Cells Using Bispecific Antibodies. *Adv. Healthcare Mater.* **2019**, *8*, 1801607.

17. Cui, J.; Alt, K.; Ju, Y.; Gunawan, S. T.; Braunger, J. A.; Wang, T.-Y.; Dai, Y.; Dai, Q.; Richardson, J. J.; Guo, J.; Björnmalm, M.; Hagemeyer, C. E.; Caruso, F. Ligand-Functionalized Poly(ethylene glycol) Particles for Tumor Targeting and Intracellular Uptake. *Biomacromolecules* **2019**, *20*, 3592–3600.

18. Ju, Y.; Kelly, H. G.; Dagley, L. E.; Reynaldi, A.; Schlub, T. E.; Spall, S. K.; Bell, C. A.; Cui, J.; Mitchell, A. J.; Lin, Z.; Wheatley, A. K.; Thurecht, K. J.; Davenport, M. P.; Webb, A. I.; Caruso, F.; Kent, S. J. Person-Specific Biomolecular Coronas Modulate Nanoparticle Interactions with Immune Cells in Human Blood. *ACS Nano* **2020**, DOI: 10.1021/acsnano.0c06679.

19. Pelaz, B.; Alexiou, C.; Alvarez-Puebla, R. A.; Alves, F.; Andrews, A. M.; Ashraf, S.; Balogh, L. P.; Ballerini, L.; Bestetti, A.; Brendel, C.; Bosi, S.; Carril, M.; Chan, W. C. W.; Chen, C.; Chen, X.; Chen, X.; Cheng, Z.; Cui, D.; Du, J.; Dullin, C.; Escudero, A.; Feliu, N.; Gao, M.; George, M.; Gogotsi, Y.; Grünweller, A.; Gu, Z.; Halas, N. J.; Hampp, N.; Hartmann, R. K.; Hersam, M. C.; Hunziker, P.; Jian, J.; Jiang, X.; Jungebluth, P.; Kadhiresan, P.; Kataoka, K.; Khademhosseini, A.; Kopeček, J.; Kotov, N. A.; Krug, H. F.; Lee, D. S.; Lehr, C.-M.; Leong, K.

W.; Liang, X.-J.; Ling Lim, M.; Liz-Marzán, L. M.; Ma, X.; Macchiarini, P.; Meng, H.; Möhwald, H.; Mulvaney, P.; Nel, A. E.; Nie, S.; Nordlander, P.; Okano, T.; Oliveira, J.; Park, T. H.; Penner, R. M.; Prato, M.; Puntes, V.; Rotello, V. M.; Samarakoon, A.; Schaak, R. E.; Shen, Y.; Sjöqvist, S.; Skirtach, A. G.; Soliman, M. G.; Stevens, M. M.; Sung, H.-W.; Tang, B. Z.; Tietze, R.; Udugama, B. N.; VanEpps, J. S.; Weil, T.; Weiss, P. S.; Willner, I.; Wu, Y.; Yang, L.; Yue, Z.; Zhang, Q.; Zhang, Q.; Zhang, X.-E.; Zhao, Y.; Zhou, X.; Parak, W. J. Diverse Applications of Nanomedicine. *ACS Nano* **2017**, *11*, 2313–2381.

20. Dai, Y.; Guo, J.; Wang, T.-Y.; Ju, Y.; Mitchell, A. J.; Bonnard, T.; Cui, J.; Richardson, J. J.; Hagemeyer, C. E.; Alt, K.; Caruso, F. Self-Assembled Nanoparticles from Phenolic Derivatives for Cancer Therapy. *Adv. Healthcare Mater.* **2017**, *6*, 1700467.

21. Ju, Y.; Cui, J.; Müllner, M.; Suma, T.; Hu, M.; Caruso, F. Engineering Low-Fouling and pH-Degradable Capsules through the Assembly of Metal–Phenolic Networks. *Biomacromolecules* **2015**, *16*, 807–814.

22. Ju, Y.; Cui, J.; Sun, H.; Müllner, M.; Dai, Y.; Guo, J.; Bertleff-Zieschang, N.; Suma, T.; Richardson, J. J.; Caruso, F. Engineering Metal-Phenolic Capsules Show Tunable Targeted Delivery to Cancer Cells. *Biomacromolecules* **2016**, *17*, 2268–2276.

23. Besford, Q. A.; Ju, Y.; Wang, T.-Y.; Yun, G.; Cherepanov, P.; Hagemeyer, C. E.; Cavalieri, F.; Caruso, F. Self-Assembled Metal–Phenolic Networks on Emulsions as Low-Fouling and pH-Responsive Particles. *Small* **2018**, *14*, 1802342.

24. Ejima, H.; Richardson, J. J.; Liang, K.; Best, J. P.; van Koeverden, M. P.; Such, G. K.; Cui, J.; Caruso, F. One-Step Assembly of Coordination Complexes for Versatile Film and Particle Engineering. *Science* **2013**, *341*, 154.

25. Lin, G.; Rahim, M. A.; Leeming, M. G.; Cortez-Jugo, C.; Besford, Q. A.; Ju, Y.; Zhong, Q.-Z.; Johnston, S. T.; Zhou, J.; Caruso, F. Selective Metal–Phenolic Assembly from Complex Multicomponent Mixtures. *ACS Appl. Mater. Interfaces* **2019**, *11*, 17714–17721.

26. Zhou, J.; Lin, Z.; Ju, Y.; Rahim, M. A.; Richardson, J. J.; Caruso, F. Polyphenol-Mediated Assembly for Particle Engineering. *Acc. Chem. Res.* **2020**, *53*, 1269–1278.

27. Poon, C.; He, C.; Liu, D.; Lu, K.; Lin, W. Self-Assembled Nanoscale Coordination Polymers Carrying Oxaliplatin and Gemcitabine for Synergistic Combination Therapy of Pancreatic Cancer. *J. Controlled Release* **2015**, *201*, 90–99.

28. Faria, M.; Björnmalm, M.; Thurecht, K. J.; Kent, S. J.; Parton, R. G.; Kavallaris, M.; Johnston, A. P. R.; Gooding, J. J.; Corrie, S. R.; Boyd, B. J.; Thordarson, P.; Whittaker, A. K.; Stevens, M. M.; Prestidge, C. A.; Porter, C. J. H.; Parak, W. J.; Davis, T. P.; Crampin, E. J.; Caruso, F. Minimum Information Reporting in Bio–Nano Experimental Literature. *Nat. Nanotechnol.* **2018**, *13*, 777–785.

29. Wei, B.; Wang, S.; Song, H.; Liu, H.; Li, J.; Liu, N. A Review of Recent Progress in Preparation of Hollow Polymer Microspheres. *Pet. Sci.* **2009**, *6*, 306–312.

30. Ahangaran, F.; Navarchian, A. H.; Picchioni, F. Material Encapsulation in Poly(methyl methacrylate) Shell: A Review. *J. Appl. Polym. Sci.* **2019**, *136*, 48039.

31. Guo, J.; Richardson, J. J.; Besford, Q. A.; Christofferson, A. J.; Dai, Y.; Ong, C. W.; Tardy, B. L.; Liang, K.; Choi, G. H.; Cui, J.; Yoo, P. J.; Yarovsky, I.; Caruso, F. Influence of Ionic Strength on the Deposition of Metal–Phenolic Networks. *Langmuir* **2017**, *33*, 10616–10622.

32. Behzadi, S.; Serpooshan, V.; Tao, W.; Hamaly, M. A.; Alkawareek, M. Y.; Dreaden, E. C.; Brown, D.; Alkilany, A. M.; Farokhzad, O. C.; Mahmoudi, M. Cellular Uptake of Nanoparticles: Journey Inside the Cell. *Chem. Soc. Rev.* **2017**, *46*, 4218–4244.

33. Kato, Y.; Ozawa, S.; Miyamoto, C.; Maehata, Y.; Suzuki, A.; Maeda, T.; Baba, Y. Acidic Extracellular Microenvironment and Cancer. *Cancer Cell Int.* **2013**, *13*, 89.

34. Riemann, A.; Ihling, A.; Thomas, J.; Schneider, B.; Thews, O.; Gekle, M. Acidic Environment Activates Inflammatory Programs in Fibroblasts via a cAMP–MAPK Pathway. *Biochim. Biophys. Acta, Mol. Cell Res.* **2015**, *1853*, 299–307.

35. Casey, J. R.; Grinstein, S.; Orlowski, J. Sensors and Regulators of Intracellular pH. *Nat. Rev. Mol. Cell Biol.* **2010**, *11*, 50–61.

36. Martinez-Finley, E. J.; Gavin, C. E.; Aschner, M.; Gunter, T. E. Manganese Neurotoxicity and the Role of Reactive Oxygen Species. *Free Radicals Biol. Med.* **2013**, *62*, 65–75.

Scheme 1. Synthesis of PEG-gallol/Mn^{II} NPs with tunable size and morphology by metal–phenolic coordination within water-in-oil emulsions.

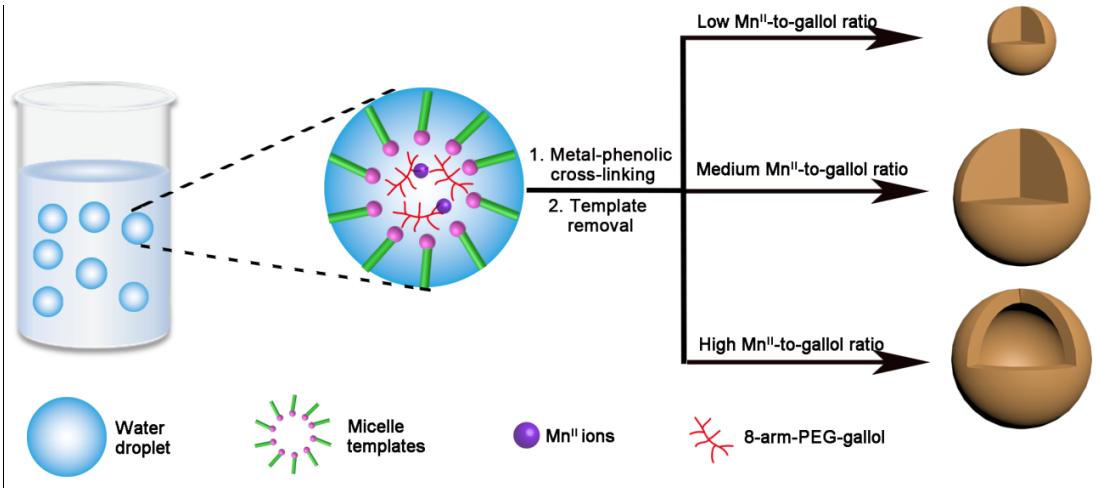

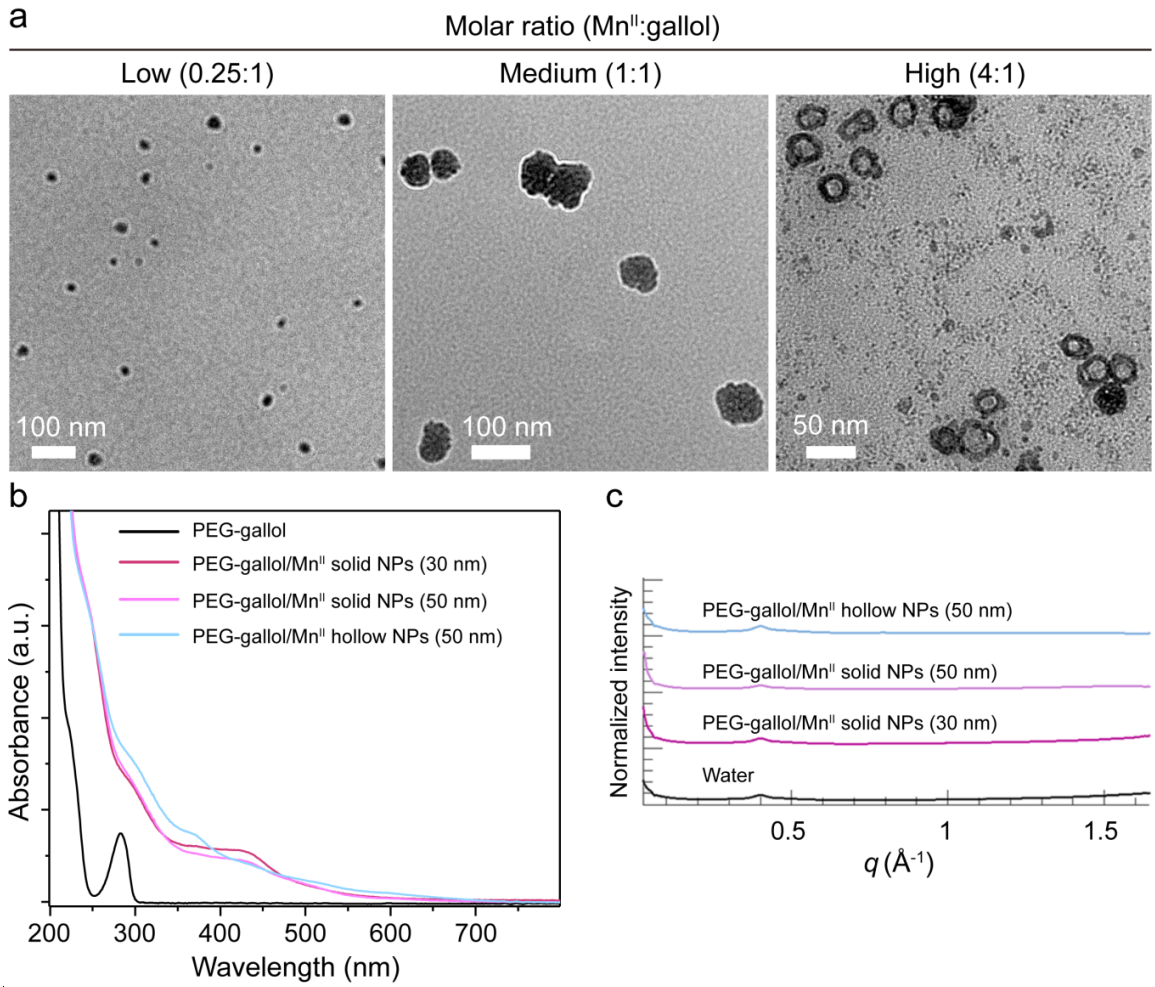

Figure 1. Characterization of different PEG-gallol/Mn^{II} NPs obtained from different Mn^{II}:gallol ratios (0.25:1, 1:1, 4:1): (a) TEM images of different PEG-gallol/Mn^{II} NPs; (b) UV–vis spectra of PEG-gallol and different PEG-gallol/Mn^{II} NPs; and (c) XRD patterns of water and different PEG-gallol/Mn^{II} NPs.

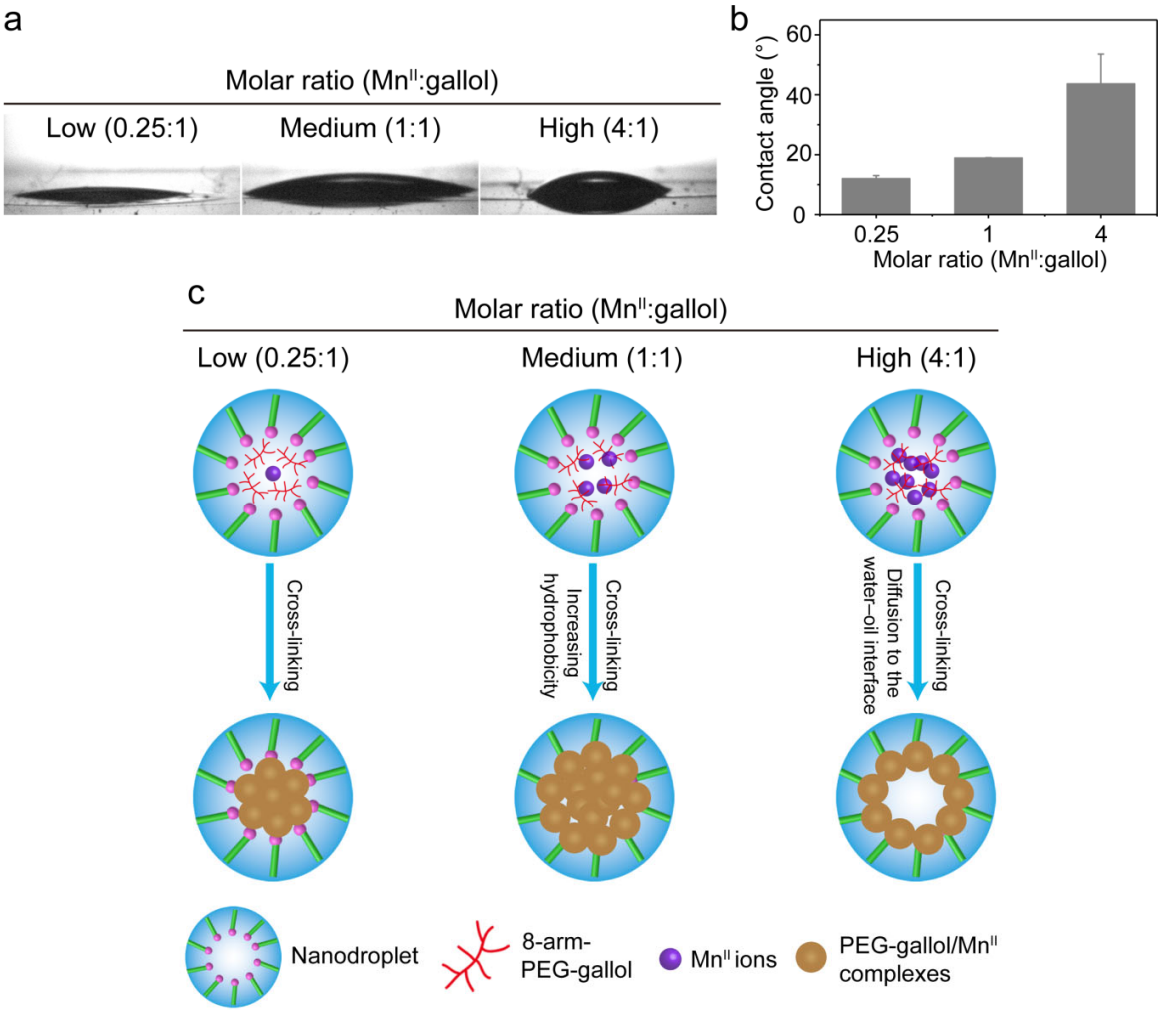

Figure 2. Contact angles of the PEG-gallol/Mn^{II} complexes and suggested mechanism of PEG-gallol/Mn^{II} NP formation. (a) Photographs of water droplets on glass coated with PEG-gallol/Mn^{II} complexes obtained at different Mn^{II}:gallol ratios and (b) the corresponding measured contact angles. (c) Schematic illustration of the mechanism of formation of the different PEG-gallol/Mn^{II} NPs, i.e., small solid NPs, large solid NPs, and large hollow NPs, by varying the Mn^{II} concentration. Increasing the Mn^{II} concentration results in an increase in the degree of cross-linking between PEG-gallol and Mn^{II}, thus making the MPN complexes more hydrophobic. This allows the complexes to diffuse toward the water–oil interface.

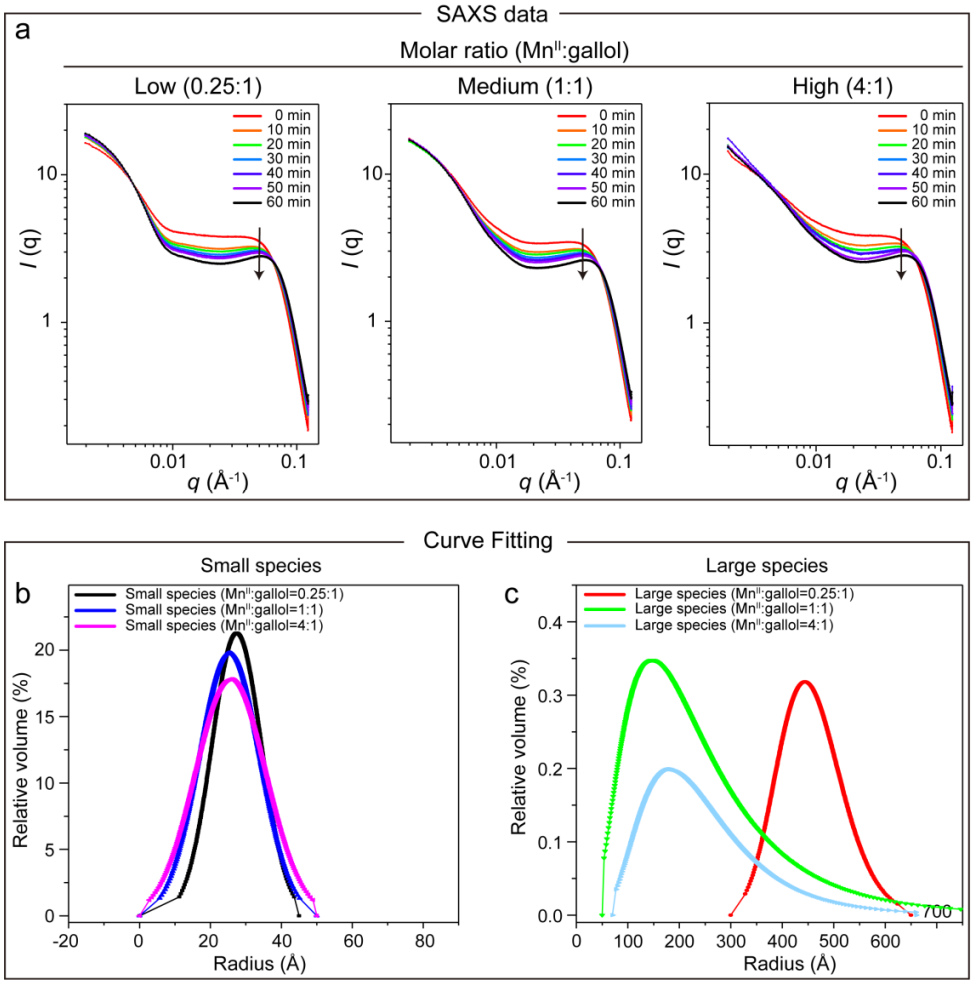

Figure 3. (a) In situ SAXS monitoring studies of particle evolution at different Mn^{II}:gallol ratios that is 0.25:1 (low ratio), 1:1 (medium ratio), and 4:1 (high ratio). (b, c) Igor 6 fitting analysis showing the relative volume of small (b) and large (c) species (PEG-gallol/Mn^{II} complexes) in the emulsions.

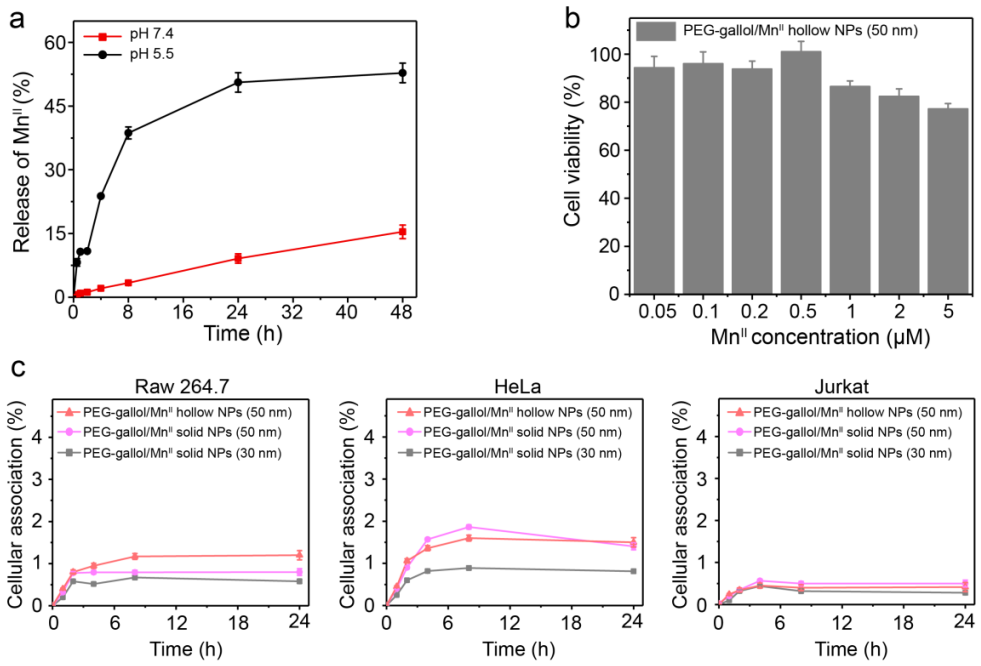

Figure 4. Stability, cytotoxicity, and low-fouling properties of PEG-gallol/Mn^{II} NPs. (a) Influence of pH on the stability of the PEG-gallol/Mn^{II} hollow NPs (50 nm) via monitoring the release of Mn^{II} ions in PBS at pH values of 7.4 and 5.5. (b) Viability of RAW 264.7 cells treated with PEG-gallol/Mn^{II} hollow NPs (50 nm) at varying concentrations. (c) Cellular association of different PEG-gallol/Mn^{II} NPs after incubation for 24 h with RAW 264.7, HeLa, or Jurkat cell lines.

Table of Contents (TOC) graphic